

Sensitivity of the Dynamic Response of Monopile-Supported Offshore Wind Turbines to Structural and Foundation Damping

Casey M. Fontana¹, Wystan Carswell¹, Sanjay R. Arwade¹, Don J. DeGroot¹ and Andrew T. Myers²

¹*Department of Civil and Environmental Engineering, University of Massachusetts Amherst, 130 Natural Resources Road, Amherst, Massachusetts 01003, USA*

²*Department of Civil and Environmental Engineering, Northeastern University, 360 Huntington Avenue, Boston, MA 02115*

Received 02/10/2015; Accepted 30/10/2015

ABSTRACT

The prediction of ultimate and fatigue demands for the design of offshore wind turbines (OWTs) requires accurate simulation of the dynamic response of OWTs subject to time-varying wind and wave loads. The magnitude of damping in an OWT system significantly influences the dynamic response, however, some sources of damping, such as foundation damping, are not explicitly considered in design guidelines and may increase damping significantly compared to commonly assumed values in design. Experimental and analytical studies have estimated the magnitude of foundation damping to be between 0.17% and 1.5% of critical, and this paper investigates how increased damping within this range affects load maxima and fatigue damage for a hypothetical 5MW OWT subjected to a variety of wind, wave, and operational conditions. The paper shows that increased damping effects the greatest percentage reduction of ultimate moment demands and fatigue damage when the OWT rotor is parked and feathered. In such cases, the aerodynamic damping is relatively low, allowing for additional damping from the foundation to account for a relatively larger proportion of the total system damping. Incorporating foundation damping in design guidelines may lead to more efficient structures, which is a crucial factor in overcoming the high cost barrier associated with offshore wind development.

Keywords: foundation damping, offshore wind, monopiles

I. INTRODUCTION

The growing demand for renewable energy sources has led to the construction of many onshore wind farms in the U.S. In 2013, these farms accounted for 4.5% of the nation's annual electricity usage (U.S. Department of Energy 2015). The U.S. Department of Energy has declared a national goal of generating 20% of the nation's electricity from renewable sources by 2030 and has stated that the least expensive way to achieve this goal includes significant development of offshore wind farms (U.S. Department of Energy 2015). Offshore wind farms have several advantages compared to onshore wind farms including the potential to install larger turbines with higher capacities in locations with stronger and steadier winds and closer proximity to electricity demand centers. While these benefits are important, there are also many additional challenges compared to onshore wind, one of which is the presence of wave loading which can have significant power spectral density at frequencies near the natural frequency of the OWT system. Moreover, it is noted that the foundation of a typical offshore wind turbine is relatively more expensive, accounting for 27% of the initial capital costs as compared to a typical onshore foundation which accounts for 16% (International

*Corresponding Author: E-mail address: cfontana@umass.edu

Renewable Energy Agency 2012). The relative expense of the support structure underscores the importance of minimizing structural weight to reduce both material and construction costs. However, design must satisfy resonance avoidance requirements in addition to strength and stiffness requirements (Myers et al. 2015). Damping is a primary factor in counteracting load amplification due to resonance, therefore it is important to reliably estimate the magnitudes of each source of damping in the system. Of these sources, it is arguable that the least is known about foundation damping, which originates from the interaction of the foundation and the soil. Examples in the literature suggest that foundation damping can contribute up to 1.5% of critical damping (Versteijlen et al. 2011). Despite the significance of this source of damping, current design guidelines do not provide a method for estimating it and it is often neglected in structural design, which may result in higher than necessary costs for the support structure.

2. PROBLEM STATEMENT

The purpose of this study is to estimate the effect of foundation damping on structural demands for a wide range of wind, wave, and operating conditions. Quantifying the significance of this effect is an important step in the decision of whether design specifications should allow inclusion of foundation damping in load analysis and whether developers and designers should invest in experimental and analytical methods to estimate the magnitude of foundation damping for a particular site and structure.

Total system damping consists of multiple sources, including aerodynamic damping, hydrodynamic damping, structural damping, foundation damping, and sometimes tuned mass damping (TMD). For linear modal damping, the total system damping ratio can be defined as the summation of damping from each source,

$$\zeta_1 = \zeta_{structural} + \zeta_{TMD} + \zeta_{aero} + \zeta_{hydro} + \zeta_{foundation} \quad (1)$$

where ζ_1 is the total system damping ratio for the first bending mode, $\zeta_{structural}$ is the hysteretic damping ratio for the structural material, ζ_{TMD} is the oscillating tuned mass damping ratio, ζ_{aero} is the aerodynamic damping ratio, ζ_{hydro} is the wave making radiation and viscous hydrodynamic damping ratio, and $\zeta_{foundation}$ is the foundation damping ratio (Damgaard and Andersen 2012). Of these sources, foundation damping properties are particularly difficult to estimate due to the non-uniformity of soil, its complex nonlinear behavior under even moderate loading, and the difficulty of obtaining detailed site characterization data. Carswell et al. (2015) investigated the significance of foundation damping on monopile-supported OWTs subjected to extreme storm loading using a linear elastic two-dimensional finite element model. This paper investigates how consideration of foundation damping through an increase in the overall structural damping affects both load maxima and fatigue damage accumulation for an example monopile-supported OWT.

3. METHODS

This investigation is structured as a parameter study with the total system damping ratio ζ_1 being the varied parameter and the peak structural demand and fatigue damage being the response quantities of interest. By formulating the problem as a parameter study it is possible to identify and illustrate trends in the effect of damping on dynamic response and to provide guidance for further, more detailed investigation of foundation damping effects. Here, an example monopile-supported OWT is analyzed dynamically for peak mudline bending moment and fatigue damage accumulation for wind and wave conditions ranging from mild to extreme and for damping ratios that cover the range of plausible contributions from the foundation system. In this section, details are provided about the structural model and software employed by this study and the input and outputs considered.

3.1. Models and software

3.1.1. Simulation software

OWT behavior is analyzed for a 5 MW reference turbine using the National Renewable Energy Laboratory's (NREL) open-source wind turbine simulation software FAST (Jonkman and Buhl Jr. 2005), which is a dynamic nonlinear analysis program that can model structural loads caused by the stochastic environment (wind and waves) and mechanical load effects from turbine operation. Details about modeling assumptions in FAST are available in the software documentation, but the software features that are particularly relevant to this study are summarized here:

1. Stochastic time and spatially varying three-dimensional wind fields.
2. Calculation of aerodynamic forces using blade element momentum theory.
3. Stochastic linear irregular wave time histories.
4. Calculation of hydrodynamic forces using the Morison equation.
5. Four degree of freedom modal analysis of the monopile/tower support structure including P- Δ effect.

3.1.2. Reference Turbine

The NREL 5 MW reference turbine is used for the OWT model due to its prevalence in the field of offshore wind energy research. This turbine is promulgated for use by the research community and is reflective of the properties of a generic utility-scale turbine (Jonkman et al. 2009). Properties of the turbine are provided in Table 1 and Figure 1. A monopile-supported foundation is considered

Table 1. Gross properties for the NREL 5 MW reference offshore wind turbine (Jonkman et al. 2009)

Property	Value/description
Rating	5 MW
Rotor Orientation, Configuration	Upwind, 3 Blades
Control	Variable Speed, Collective Pitch
Rotor, Hub Diameter	126 m, 3 m
Hub Height	90 m
Cut-In, Rated, Cut-Out Wind Speed	3 m/s, 11.4 m/s, 25 m/s
Rotor Mass	110,000 kg
Nacelle Mass	240,000 kg
Tower Mass	347,460 kg
Coordinate Location of Overall Center of Mass	(-0.2 m, 0.0 m, 64.0 m)
Natural frequency	0.27 Hz

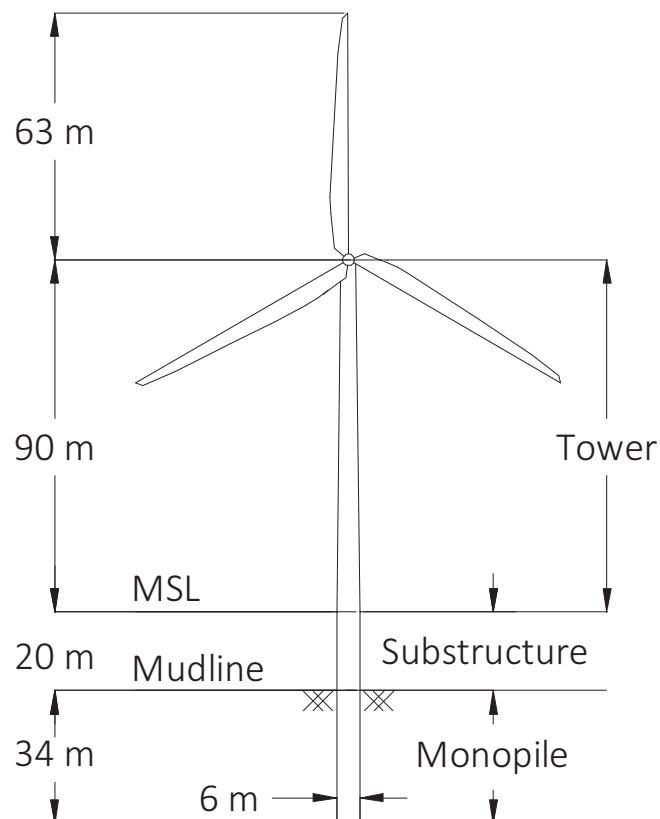


Figure 1. Schematic of the NREL 5MW with fixed bottom and supported by a monopile foundation (Carswell et al. 2015). MSL = Mean Sea Level

because it best represents current practice – a majority (65%) of installed OWTs utilize monopile-type foundations, and it is anticipated that they will continue to dominate the industry (Macaskill and Mitchell 2013).

Monopiles can be constructed in shallow water depths up to ~30 m (Musial and Ram 2010). The water depth considered for this study is 20 meters, a depth reflective of potential east coast installation locations (Musial and Ram 2010) and comparable to many other publications that consider the NREL 5MW reference offshore turbine.

3.1.3. Approximation of foundation damping by structural damping

Foundation damping is a dynamic property of the support conditions resulting from soil structure interaction. It is dependent on the strength and stiffness of the support and surrounding soil, and can be described as the mechanism in which energy is dissipated when cyclic motion in the soil takes place. FAST does not include the capability to model soil nonlinearity which is the source of foundation damping, therefore foundation damping is modeled with equivalent modal damping and added to the structural damping input value. In reality, foundation damping is applied as a distributed force below the mudline and is dependent on many more factors than just velocity, so this simplification results in a loss of frequency and amplitude dependence that appears in detailed geotechnical modeling of foundation dynamics. However, modeling the role of foundation damping in the dynamic response of an OWT through an increase in the total structural damping modeled in FAST allows for efficient simulation of OWT response in this parameter study. In addition, this simplification is reasonable because the emphasis of this study is placed on effects of the increase in system damping due to increased foundation damping, not on the foundation damping values themselves.

The structural damping value in FAST is inputted directly by the user, while hydrodynamic damping (ζ_{hydro}) and aerodynamic damping (ζ_{aero}) values are generated through dynamic analyses in FAST. Tuned mass damping (ζ_{TMD}) is 0% because the NREL 5MW reference offshore turbine does not include a tuned mass damper. Structural damping in FAST is modeled with implementation of simplified Rayleigh damping by the designation of four damping ratios corresponding to the 1st and 2nd fore-aft (FA) modes and the 1st and 2nd side-side (SS) modes. The model includes a structural damping ratio set equal to a constant value of 1.0%, which is a standard value for the NREL 5 MW OWT supported by a steel tower and monopile (Jonkman et al. 2009) and represents the inherent damping of the structural material. The literature on the magnitude of foundation damping determined via free vibration and log decrement analyses suggests that it can provide a contribution of 0.17%–0.28% of critical damping when estimated numerically (Carswell et al. 2015) and 0.25%–1.5% when back-calculated experimentally (Shirzadeh et al. 2013; Versteijlen et al. 2011). It is noted that these estimates of foundation damping contribution are highly sensitive to modeling assumptions and experimental conditions, meaning that true foundation damping contributions could be different due to variation in soil properties and many other factors. This range of foundation damping values stated in the literature has already been converted equivalent modal damping, therefore a range of foundation damping ratio inputs between 0% and 2% added to the structural damping value are analyzed in this study.

Numerical experiments by the authors have indicated that, due to complexities in the way the tower mode shapes and the added mass of the rotor-nacelle-assemble are considered in FAST, the target structural damping ratios specified in the FAST input files are not realized when the resulting model is exercised in a free vibration analysis. Rather, the model exhibits substantially less damping than is specified in the input files. Figure 2 shows the relationship between the input structural damping ratio and that calculated using the log decrement method applied to the tower-top displacement in a free vibration analysis executed with no external wind or wave loading and with the rotor and blades parked and feathered. The figure shows that the effective structural damping in the model is approximately 30%–40% of that specified in the input file. Even though the model includes additional damping due to the explicit modeling of aerodynamic and hydrodynamic forces which resist structural motion, these additional sources are expected to be minimal since the rotor and blades are parked and feathered and since there is no external wind or wave loading.

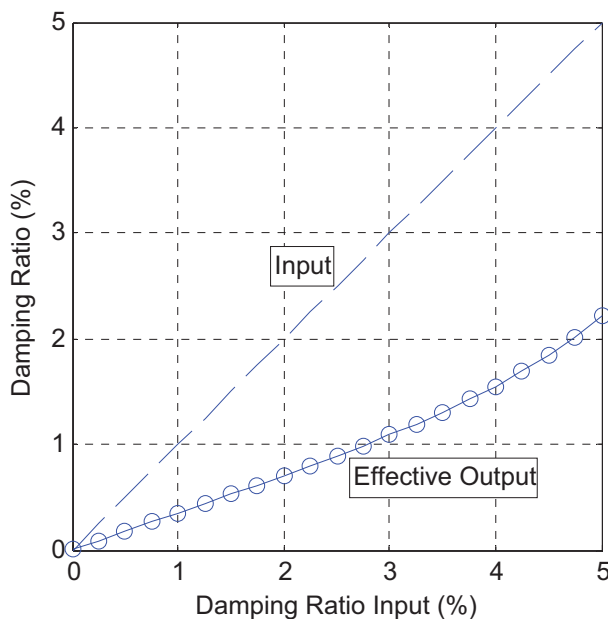


Figure 2. Inconsistencies in FAST between the damping ratio specified as input and that calculated based on a log decrement analysis of the tower top displacement subjected to free vibration

Therefore, to account for this inconsistency and still model the full range of foundation damping ratios between 0 and 2%, a range of structural damping ratios between 1% (i.e., structural damping only) and 5% (i.e., 1% structural damping plus approximately two times the maximum foundation damping of 2%) is specified as input into the FAST analyses.

3.2. Summary of Input Parameters

A summary of input parameters considered in this study is provided in Table 2. The first three rows in the table provide the range of damping ratio, wind speed, and wave height selected for the parameter study while the remaining rows give parameters that are held constant across all simulations.

Selected wind speeds are chosen because they correspond to important operational states for the NREL 5 MW turbine: the cut-in speed (3 m/s) is the minimum speed at which the turbine operates, the rated speed (11.4 m/s) is the wind speed at peak power generation, and the cut-out speed (25 m/s) is the maximum speed at which the turbine operates. The 30 m/s wind speed is included in the study to examine non-operating conditions when the turbine is parked (blade movement restricted by brake) and blades are feathered. A turbulence intensity of 11% is chosen because it is reflective of typical offshore conditions and is commonly used in OWT research.

The lower limit of significant wave height range (0 m) is chosen to analyze the case of no wave loading, while the upper limit of the significant wave height range (8 m) is chosen based on breaking wave criteria, where $H/d = 0.78$ is generally considered to define the onset of breaking waves (Stansby, Stallard, and Devaney 2013). For the 20 m water depth in this research, the

Table 2. Summary of FAST input parameters

Parameter	Value/Description
Damping ratios	1%, 2%, 3%, 4%, 5%
Wind speeds, V	3 m/s, 11.4 m/s, 25 m/s, 30 m/s
Significant wave heights, H_s	0 m, 2 m, 4 m, 6 m, 8 m
Water depth	20 m
Platform model	Fixed bottom offshore
Wind turbulence model	IEC Kaimal
Turbulence intensity	11%
Incident wave kinematics model	JONSWAP/Pierson-Moskowitz spectrum (linear irregular)
Wind-wave alignment	Co-directional

corresponding breaking wave height is 15.6 m, which becomes the limiting maximum value of wave height. Maximum wave height is defined by $1.86H_s$ (DNV 2013), therefore the significant wave height for the onset of breaking waves in 20 m water depth is approximately 8 m.

Wave period is calculated according to IEC standard 61400, given by:

$$11.1 \times \sqrt{\frac{H_s}{g}} \leq T \leq 14.3 \times \sqrt{\frac{H_s}{g}} \quad (2)$$

where T is the wave period, H_s is the significant wave height, and g is gravity (IEC 61400-3 2009). The lower limit factor of 11.1 is used in this study to maximize the wave power spectral density associated with the natural frequency of the structure (0.27 Hz). This models the wave loading within this range that is expected to cause the largest loads and to have the most waves impacting the structure in a given time, thereby maximizing fatigue damage estimates. These calculated values of wave periods are used for the peak spectral period inputs in FAST.

Six 1-hour simulations are completed for each input value of damping ratio - 1, 2, 3, 4, and 5% - and for each combination of wind speed and wave height in accordance with IEC standards (IEC 61400-3 2009). Each of the 6 simulations uses a different set of seeds to initialize the random number generators which initiate the stochastic wind and wave histories. The same 6 sets of seeds are used for each damping ratio and for each combination of wind speed and wave height to remove estimation variability from the comparison of dynamic response across wind, wave, and damping conditions. For each combination of wind speed and wave height conditions, 30 simulations are carried out (5 damping ratios and 6 seed sets), resulting in a total of 600 1-hr simulations in FAST.

3.3. Maximum load definition

For simplicity, the maximum load considered in this study is the resultant mudline bending moment, calculated by combining the fore-aft (FA) and side-side (SS) moments provided in the FAST output. In particular, resultant moment time histories are generated by calculating the vector sum of the FA and SS moment output values from FAST at every time instant, as shown in Figure 3.

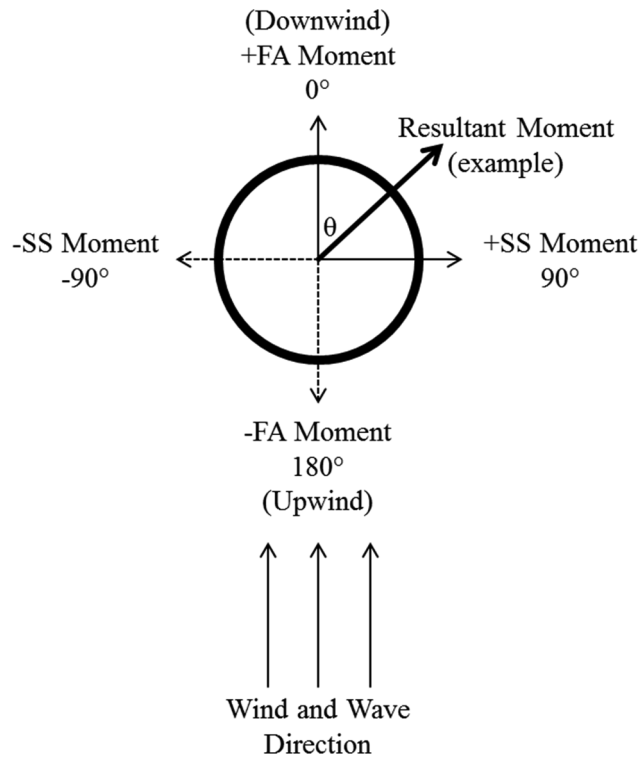


Figure 3. Top view of monopile cross-section at the mudline showing the fore-aft (FA) and side-to-side (SS) direction and an example direction of the resultant moment

For each combination of wind speed, wave height, and damping ratio, the maximum resultant moment is calculated for each of the 6 independent simulations (corresponding to different random number seeds) and the peak response is taken to be the average of those 6 maxima. This average is typically used in industry and provides a more stable estimator of the extreme loads than would the maximum of a single simulation.

3.4. Fatigue Damage

The second portion of the research investigates the effects of damping on fatigue damage accumulation in the cross-section located at the mudline of the monopile. Fatigue damage is calculated by selecting a material stress-lifetime (S-N) curve that best models the turbine's cross-section at the mudline (Veritas 2005), generating combined bending/axial stress time histories from FAST output for circumferential orientations spaced at 5 degree increments around the base, executing rainflow cycle counting, applying the Goodman correction for mean stress effects (Manwell, McGowan, and Rogers 2002), and using the Palmgren-Miner rule (Veritas 2005) to compute the fatigue damage during the one hour simulations described above. This fatigue analysis gives estimates of the accumulated fatigue damage that occurs during a one hour simulation under specified wind speed, wave height, and damping ratio and provides guidance on how foundation damping may mitigate fatigue damage over a wide range of environmental conditions.

Fatigue damage analysis is performed following the Recommended Practice DNV-RP-C203 (Veritas 2005), which is valid for examining fatigue damage in the high cycle region with stress values up to 550 MPa (DNV 2005). The use of this practice is appropriate here given the high number of cycles associated with the environmental loading on OWTs and the stress magnitudes calculated by FAST. The DNV Recommended Practice states that accumulated fatigue damage may be calculated based on the stress-life fatigue approach under the assumption of linear cumulative damage (Palmgren-Miner rule, Veritas 2005), which states that,

$$D = \sum_{i=1}^k \frac{n_i}{N_i} \leq \eta \quad (3)$$

where D is accumulated fatigue damage, k is the number of stress range blocks, n_i is the number of stress cycles in stress range block i , N_i is the number of cycles to failure at stress range corresponding to block i , and η is the usage factor (DNV 2005).

3.4.1. Selection of a stress-life curve

The S-N curve considered here is the C1 curve for offshore steel structures in seawater with cathodic protection (Veritas 2005). This curve is appropriate for the tubular steel pipe connecting the turbine to the foundation at the mudline, assuming the connection is a two-sided circumferential butt weld dressed flush (Veritas 2005). The curve is governed by

$$\log N = \log \bar{a} - m \log \Delta\sigma \quad (4)$$

where N is the predicted number of cycles to failure for stress range $\Delta\sigma$, $\log \bar{a}$ is the intercept between the log N-axis and the S-N curve, m is the negative inverse slope of the S-N curve, and $\Delta\sigma$ is stress range. For the C1 curve in the range $N \leq 10^6$ cycles, the values for $\log \bar{a}$ and m are 12.0 and 3.0 respectively. For $N > 10^6$ cycles, the values for $\log \bar{a}$ and m are 16.1 and 5.0, respectively. The design S-N curve is based on the mean-minus-two-standard-deviation curve for relevant experimental data, and is therefore associated with a 97.7% probability of survival (DNV 2005). As shown in this curve, larger amplitude stresses correspond to shorter lifespans due to their nonlinearly larger effect on fatigue damage accumulation.

3.4.2. Stress time history

The total stress in the base at any time instant, σ_{total} , is calculated by the sum of the bending stress and axial stress,

$$\sigma_{total}(t, \theta) = \sigma_b(t, \theta) + \sigma_n \quad (5)$$

where σ_b is the bending stress caused by the resultant bending moment, t is time, θ is the angle from the fore-aft downwind direction as shown in Figure 3 and σ_n is the constant axial stress (15.1 MPa) due to the self-weight of the combined rotor nacelle assembly (RNA), tower, and monopile. Note that the axial stress induced by gravity is considered to be time invariant and constant around the circumference of the monopile, and that this assumption neglects nonlinear effects and the small bending moment and resulting stress induced by the small eccentricity between the RNA center of mass and the centerline of the tower. The resultant bending stress is calculated at 5° increments around the base of the turbine. It is necessary to calculate individual stress time histories at incremental points because damage varies with circumferential orientation around the base. Relevant properties of the monopile's tubular steel pipe at the mudline are summarized in Table 3.

Table 3. Base properties of NREL 5-MW turbine used for stress calculations (Jonkman et al. 2009)

Turbine Base Property	Value
Outer diameter	6 m
Wall thickness	0.027 m
Moment of inertia	2.26 m ⁴
Cross sectional area	0.507 m ²
Self-weight at base	7.64 MN

3.4.3. Rainflow counting and mean stress effects

Due to the high variability of the turbulent winds and irregular waves modeled in FAST, the total stress time histories computed display a large range in cycle amplitude. The MATLAB rainflow counting function, *rainflow*, is used to extract cycle counts, amplitudes, and means from each stress time history.

Most cycles in the operating cases have nonzero mean stresses because of the nonzero average thrust acting on the rotor. The C1 S-N curve from Recommended Practice C203 is generated based on fully reversed stress cycles with zero mean stress. To consider mean stress effects in the prediction of fatigue damage, the Goodman relationship (Manwell et al. 2002) is used, which states

$$\frac{\sigma_a}{\sigma'_e} + \frac{\sigma_m}{\sigma_u} = 1 \quad (6)$$

where σ_a is the stress amplitude, σ_m is the mean stress, σ_u is the ultimate strength of the steel (450 MPa (DNV 2013)), and σ'_e is effective stress amplitude. The Goodman effective stress amplitude, σ'_e , is the equivalent stress amplitude for fully reversed zero mean stress criteria. The results from the rainflow counting are sorted by both amplitude and mean (20 by 20 binning, as recommended by DNV (2005)), and the Goodman correction is applied to each bin.

3.4.4. Average maximum fatigue damage

After pairs of effective stress amplitude and cycle count are calculated for each of the simulation runs, these pairs are used as input to the Palmgren-Miner equation to calculate the fatigue damage accumulated during the simulation. Purely compressive stress cycles are generally not considered to contribute to fatigue damage. Therefore, when computing the effective stress, if the sum of the mean stress and stress amplitude of the bin is negative (i.e., if the bin's stress cycle range is entirely compressive), those cycles are not included in the Palmgren-Miner fatigue damage accumulation calculation. Effective stress amplitudes are doubled to find the effective stress range for use in the S-N curve, which is defined in terms of stress range rather than amplitude. This modified Palmgren-Miner damage equation states,

$$D = \sum_{i,j=1}^k \frac{n_{ij}}{N_{ij}} \leq \eta \quad (7)$$

where n_{ij} is the number of stress cycles at amplitude i and mean stress j , and N_{ij} is the number of cycles to failure for the Goodman effective stress range at amplitude i and mean stress j . Stress concentration factors (SCF) that may act to increase stresses are neglected here since the emphasis is on comparison between fatigue damage at different damping ratios and environmental conditions, rather than on the absolute value of that fatigue damage. The same process of averaging the 6 one-hour simulations is used to find the average values of D at each 5° increment. For each combination of wind speed, wave height, and damping ratio, only the circumferential orientation of maximum damage and the associated damage value is used for comparison between cases to evaluate effects of increased damping.

4. RESULTS

As expected, increased damping is found to decrease the average maximum resultant mudline moment and the average maximum damage accumulation in all combinations of wind speed and wave height. In the following subsections detailed descriptions of these effects are given for the maximum resultant moment and fatigue damage cases.

4.1. Effects of increased damping on maximum mudline moment

Increased damping decreases the amplitude of the resultant moment in all cases, as demonstrated by a sample resultant mudline moment time history shown in Figure 4.

The maximum values of resultant moment for each case are shown in Table 4, as calculated by averaging the maxima for the 6 distinct seeds. The shading in the table indicates magnitude, as detailed in the scale provided; the smallest moments are shaded green, and the largest moments are shaded red. The largest estimate for the resultant moment at the mudline is 132 MN-m, which is about one-half of the yield moment, 260 MN-m, of the cross-section of the monopile at the mudline. This moment was estimated for all considered damping ratios for the rated wind speed (11.4 m/s, the operational speed when the average rotor thrust is largest) and the significant wave height of 8 m.

The effect of increasing damping is evaluated by calculating the percent reduction in the maximum value as compared to the value calculated for a damping ratio of 1%, as shown in Table 5. Bolded values highlight the maximum reductions for each wind speed case, and the darkness of the red and green shading indicates the magnitude of the moment and percent reduction values, respectively.

For the operational cases (wind speeds 3 m/s, 11.4 m/s, and 25 m/s), the increase in damping ratio has a small effect on moment reduction. For the non-operational cases (wind speed 30 m/s), the increase in damping ratio has up to a 17% reduction in moment. This difference in load reduction between the operational and non-operational cases is explained by aerodynamic damping. In the operational cases, where the resultant moment at any time instant is approximately in the FA

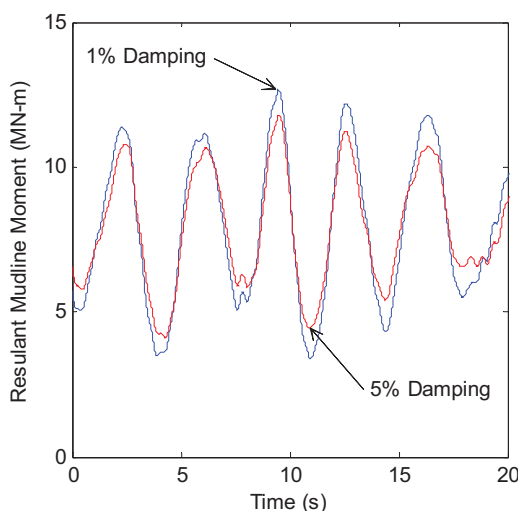


Figure 4. The effect of increasing damping from 1% to 5% on the resultant mudline moment for a wind speed of 3 m/s, a significant wave height of 2 m, and operational conditions

downwind direction (Figure 3), the aerodynamic damping in the fore-aft direction generated by the spinning blades provides a significant amount of the system's total damping, therefore changes in foundation damping have a small effect. As a point of comparison, the fore-aft aerodynamic damping ratio for the 1.5MW NREL reference turbine has been estimated to be between 3.7% and 5.4% of critical during operational conditions (Valamanesh and Myers 2014). In parked and feathered cases, the lack of aerodynamic damping allows for foundation damping to account for a greater portion of the total system damping, therefore changes in foundation damping have a larger effect on the loading.

The nature of aerodynamic damping also explains why, amongst the operating cases, the 3 m/s case sees the largest percent reduction as compared to the 11.4 and 25 m/s cases. Aerodynamic damping contribution is dependent on the characteristics of the wind; for lower wind speeds like 3 m/s, less aerodynamic damping in the fore-aft direction is present, allowing foundation damping to play a stronger role in total system damping. The most aerodynamic damping is present in the fore-aft direction for the 11.4 and 25 m/s wind speed cases, therefore the resultant moment in these cases undergoes the least effect from changes in foundation damping. Magnitudes of fore-aft aerodynamic damping for different wind speeds and operational conditions can be determined via the methods described in Valamanesh and Myers (2014).

The reduction in moment due to increased damping does not vary linearly with wave height. The maximum reductions in moment occur for the 0 or 2 m significant wave height cases for all wind

Table 4. Average maximum values from six one hour-simulations for the resultant mudline moment, MN-m, for various combinations of damping ratio, wind speed, wave height and operational conditions


						
		11.5 MN-m	67 MN-m	132.2 MN-m		
		Damping Ratio, %				
		1	2	3	4	5
		Wind Speed 3 m/s (cut-in; operational)				
Significant Wave Height, m	0	11.7	11.6	11.6	11.5	11.5
	2	26.3	25.9	25.6	25.4	25.2
	4	34.6	34.2	34.0	33.8	33.7
	6	49.9	49.4	49.1	48.8	48.5
	8	63.4	63.4	63.4	63.4	63.4
		Wind Speed 11.4 m/s (rated; operational)				
Significant Wave Height, m	0	95.6	95.1	94.8	94.5	94.3
	2	102.1	101.6	101.3	101.0	100.7
	4	109.2	108.9	108.6	108.3	108.1
	6	116.2	115.9	115.7	115.5	115.3
	8	132.2	132.2	132.2	132.2	132.2
		Wind Speed 25 m/s (cut-out; operational)				
Significant Wave Height, m	0	70.6	69.7	69.0	68.5	68.1
	2	74.0	73.4	72.9	72.4	71.9
	4	77.0	76.0	75.4	75.0	74.6
	6	80.9	80.4	80.1	79.9	79.6
	8	93.9	93.4	93.0	92.8	92.6
		Wind Speed 30 m/s (parked and feathered; non-operational)				
Significant Wave Height, m	0	31.3	30.2	29.4	28.5	28.0
	2	35.3	32.8	31.3	30.2	29.2
	4	40.9	39.1	37.0	35.5	34.5
	6	53.0	50.3	48.7	47.8	47.0
	8	63.2	61.3	60.8	60.5	60.3

Table 5. Percent reduction in resultant moment as compared to value at 1% damping ratio for various combinations of damping ratio, wind speed, wave height and operational conditions.

		Damping Ratio, %				
		1	2	3	4	5
		Resultant Moment, MN-m	Percent Reduction			
		Wind Speed 3 m/s (cut-in; operational)				
Significant Wave Height, m	0	11.7	0.7%	1.3%	1.8%	2.2%
	2	26.3	1.4%	2.5%	3.4%	4.2%
	4	34.6	1.1%	1.8%	2.2%	2.5%
	6	49.9	0.8%	1.5%	2.1%	2.7%
	8	63.4	0.0%	0.0%	0.0%	0.0%
		Wind Speed 11.4 m/s (rated; operational)				
Significant Wave Height, m	0	95.6	0.5%	0.8%	1.1%	1.4%
	2	102.1	0.4%	0.8%	1.1%	1.3%
	4	109.2	0.3%	0.6%	0.8%	1.0%
	6	116.2	0.2%	0.4%	0.6%	0.8%
	8	132.2	0.0%	0.0%	0.0%	0.0%
		Wind Speed 25 m/s (cut-out; operational)				
Significant Wave Height, m	0	70.6	1.3%	2.3%	3.0%	3.6%
	2	74.0	0.9%	1.6%	2.2%	2.8%
	4	77.0	1.2%	2.1%	2.6%	3.1%
	6	80.9	0.5%	0.9%	1.2%	1.6%
	8	93.9	0.5%	0.9%	1.2%	1.4%
		Wind Speed 30 m/s (parked and feathered; non-operational)				
Significant Wave Height, m	0	31.3	3.3%	6.1%	8.8%	10.5%
	2	35.3	7.2%	11.3%	14.5%	17.3%
	4	40.9	4.5%	9.7%	13.2%	15.6%
	6	53.0	5.1%	8.0%	9.8%	11.2%
	8	63.2	2.9%	3.7%	4.2%	4.5%

speeds. This is due to the wave conditions in these cases having significant power spectral density at frequencies near the turbine’s natural frequency and blade passing frequencies. The NREL 5MW fixed bottom offshore monopile reference turbine in 20 m of water depth has a natural frequency f_n of 0.27 Hz, as determined from free vibration simulations in FAST (Carswell). The 1P and 3P blade passing frequencies, f_{1P} and f_{3P} , of the NREL 5MW are 0.20 and 0.33, respectively (ABS 2011). The wave period used for the peak spectral period input for each significant wave height is determined via eqn (2), and the associated frequency is the inverse of this value as shown in Table 6.

Table 6. Peak spectral loading frequencies for each significant wave height and the ratio of these frequencies to the NREL 5MW natural, 1P, and 3P frequencies.

Significant Wave Height, (m)	Peak Spectral Wave Loading Frequency, f_{wave} (Hz)	Frequency Ratios		
		f_{wave}/f_n	f_{wave}/f_{1P}	f_{wave}/f_{3P}
0	∞	∞	∞	∞
2	0.20	0.74	1.00	0.59
4	0.14	0.52	0.71	0.41
6	0.12	0.43	0.58	0.34
8	0.10	0.37	0.50	0.29

A frequency ratio of 1.0 corresponds to conditions in which the wave loading has a peak spectral frequency equivalent to the turbine's natural frequency or blade passing frequency. The turbine's natural frequency (0.27 Hz), 1P frequency (0.20 Hz), and 3P frequency (0.33 Hz) all fall between the peak spectral wave loading frequencies at 0 m (∞ Hz) and 2 m (0.20 Hz), which generates the most load amplification compared to other significant wave height cases. Since dynamic response of a system is most sensitive to damping near the resonant frequency (Chopra 1992), the effects of increased damping are most significant in cases where loading experiences the most amplification, when frequency ratios are closest to 1.0.

4.2. Effects of increased damping on fatigue damage accumulation

Increased damping decreases the fatigue damage accumulation in all combinations of wind speed and significant wave height. This is consistent with the reductions in mudline moment results described in the previous section, since damage is a function of moment and the resulting stress values.

4.2.1. Rainflow counting and 2D binning of total stress cycle amplitudes and means

The stochastic nature of the environmental loading from the turbulent winds and irregular waves results in significant randomness within a stress time history and significant variability between nominally identical simulations. Figure 5 shows this in total stress time history samples for nominally identical simulations.

The rainflow counting process described previously is used to decompose each stress time history into an amplitude and mean for every stress cycle. It is found that most cycles located in the FA upwind circumferential orientation on the cross-section (180° see Figure 3) for the operating cases have nonzero mean stresses, due to the presence of the non-zero thrust acting in the fore-aft direction. An example of the presence of non-zero mean stresses is shown in Figure 6.

This non-zero mean stress results from the interaction between the wind and blades when the turbine is operational; parked and feathered conditions exhibit mean stresses close to zero. Figure 6 shows a selected case in which maximum loading occurs (wind speed 11.4 m/s, significant wave height 8 m, damping ratio 1%), therefore the mean stress is significantly larger than the stress amplitude. The variations in total stress from wind turbulence and wave irregularity is minimal compared to the large constant blade-wind interaction stress inherent in peak power production conditions. An example of 2D binning used to analyze the extracted total stress cycle amplitudes and means is shown in Figure 7.

In operating cases, the mean total stress in the FA upwind circumferential orientation remained approximately the same across all wave heights. The mean stress results reflect values shown in Table 4, as mean bending stress is closely related to moment – the rated wind speed cases have the

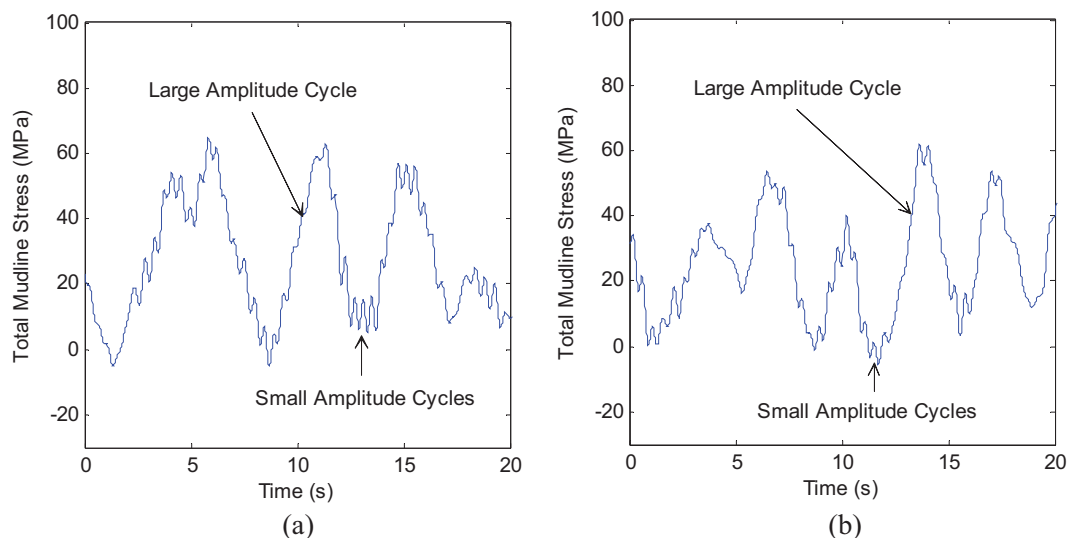


Figure 5. Variations in total stress cycle amplitude for a wind speed of 25 m/s (operational), a significant wave height of 8 m, and a damping ratio of 1% for Seed 1 (a) and Seed 2 (b)

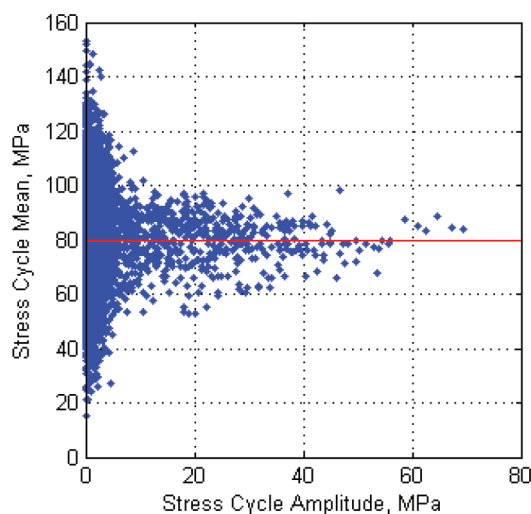


Figure 6. Total stress cycle amplitude versus stress cycle mean from rainflow counting for wind a speed of 11.4 m/s (operational), a significant wave height of 8 m, a damping ratio 1%, and 180° FA upwind circumferential orientation on the mudline cross-section of the monopile (see Figure 3) to show need for incorporation of mean stress effects

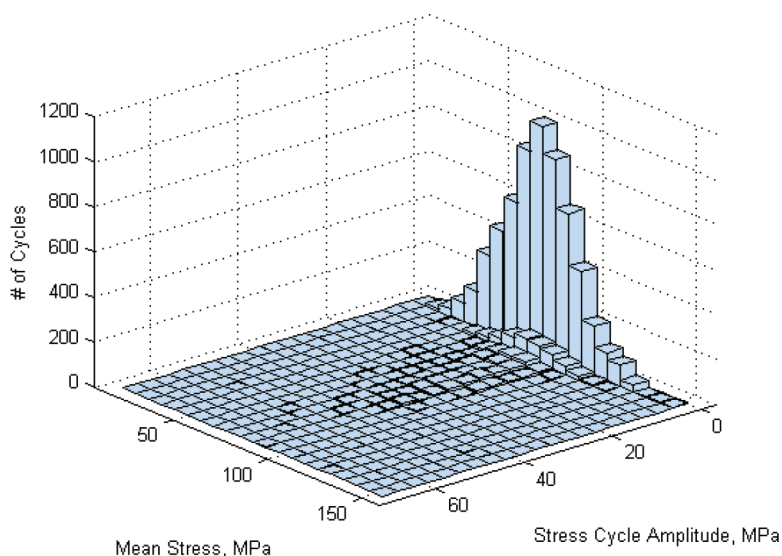


Figure 7. 2D Binning histogram of total stress amplitude bins, mean stress bins, and number of cycles in the bin for a wind speed of 11.4 m/s, a significant wave height of 8 m, a damping ratio of 1%, and 180° FA upwind circumferential orientation on the mudline cross-section of the monopile (see Figure 3)

highest magnitude mean bending stresses (~95 MPa) and the cut-in have the lowest (~10 MPa). In parked and feathered cases, the mean FA upwind bending stress magnitudes are more sensitive to wave loading due to the lack of blade-wind interaction (~8 MPa at 0 m wave height to ~16 MPa at 8 m wave height).

4.2.2. Damage accumulation for the circumferential orientation with maximum damage

The circumferential orientation of maximum damage can be seen in Table 7. A diagram showing the orientation of the angle measure is shown in Figure 3. All of the results in this section are provided for the circumferential orientation with maximum damage.

In the cut-in, rated, and cut-out wind speed cases, the FA upwind circumferential orientation (180°) is generally found to accumulate the most damage because this circumferential orientation experiences the highest mean tensile stress. Due to the blade-wind interaction, the

Table 7. Circumferential orientation of maximum damage on the mudline cross-section of the monopile. Angle reference point is provided in Figure 3

		Wind Speed, m/s			
		3	11.4	25	30
Significant Wave Height, m	0	180°	180°	-170°	90°
	2	180°	180°	-175°	90°
	4	180°	180°	-175°	165°
	6	180°	180°	-175°	180°
	8	180°	180°	-175°	180°

turbine is always bending downwind in operating cases, creating the highest tensile bending stress in the FA upwind circumferential orientation and the highest compressive stresses in the FA downwind circumferential orientation (0° , see Figure 3), as shown in Figure 8. The circumferential orientation of maximum damage favors -170° and -175° in the cut-out wind speed case due to the lack of symmetry of the blades, which becomes a more pronounced effect at high wind speed.

The lack of symmetry about zero stress in Figure 8 is due to the constant axial compressive stress and approximately constant bending stress resulting from the overturning moment acting on the rotor. Since the additional compressive axial stress acts equally in all circumferential orientations around the base, the bending stress wind and wave loading governs the circumferential orientation of maximum fatigue damage values. Additionally, entirely compressive stress cycles such as those experienced in the FA downwind circumferential orientation are not considered in the Palmgren-Miner model to contribute to fatigue damage.

In the parked and feathered cases with significant wave height equal to 0 and 2 m, the SS circumferential orientation (90°) is found to accumulate the most damage, though it should be noted that the absolute levels of damage in these cases are low due to the low wave heights. When the blades are feathered, this orientation reduces aerodynamic drag in the FA direction, while increasing drag in the SS direction, as shown in Figure 9.

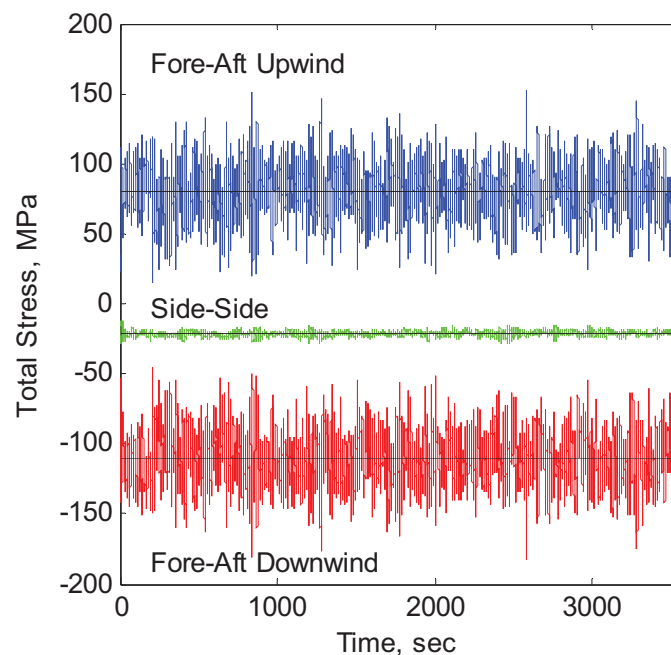


Figure 8. Total stress time histories and means of fore-aft upwind (180°), side-side (90°), and fore-aft downwind (0°) for a wind speed of 11.4 m/s, a significant wave height of 8 m, and a damping ratio of 5%

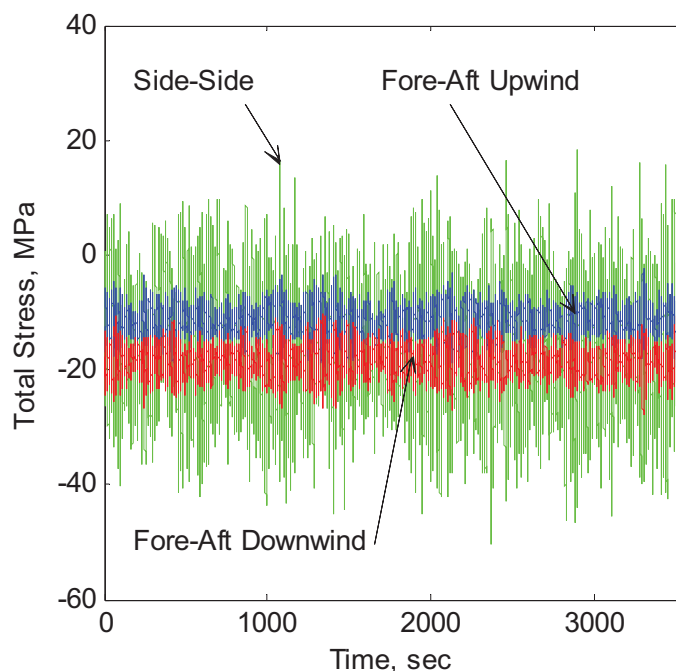


Figure 9. Total stress time histories of fore-aft upwind (180°), side-side (90°), and fore-aft downwind (0°) for a wind speed of 30 m/s, 0 m significant wave height, and a damping ratio of 5%

As wave height transitions from 0 m (as shown in Figure 9) to 8 m, the dominant source of stress shifts from aerodynamic loads in the SS direction to wave loading in the FA direction. This explains why the FA upwind circumferential orientation sees the most damage in higher wave height cases for parked and feathered conditions as shown in Table 7.

Damage accumulations based on the Palmgren-Miner rule for a 1-hour period are provided in Table 8, as calculated by averaging the 1-hour damage accumulation for the 6 distinct seeds at the circumferential orientation corresponding to maximum damage (see Table 7). The shading in the table indicates damage magnitude, as detailed in the scale provided; the smallest damage values are shaded green, and the largest damage values are shaded red. This research is focused on the effects of damping on offshore wind turbine dynamics and fatigue, therefore the 1-hour damage values are generated for comparison purposes to evaluate the reduction in damage with increased damping. These damage values cannot be compared to a usage factor, η , as specified in the Recommended Practice C203 because the usage factor is specific to a 20 year lifespan of the turbine.

When interpreting the results in Table 8, it is important to note that fatigue damage does not vary linearly with stress amplitude because the S-N curve is nonlinear, therefore the relationship between damping magnitude and damage is also nonlinear. The effect of increased damping on fatigue damage is evaluated by calculating the percent reduction in damage as compared to the damage at 1% damping ratio. The results are shown in Table 9. Bolded values highlight the maximum reductions for each wind speed case, and the darkness of the red and green shading indicates the magnitude of the damage and percent reductions, respectively.

Fatigue damage results parallel resultant mudline moment results in that the greatest effect of increased damping is seen in the parked and feathered cases (up to 69% reduction), and the least effect is seen the operating cases. This is again explained by the lack of aerodynamic damping in the parked and feathered cases, which allows for foundation damping to account for a larger fraction of total system damping. Although similar numbers of stress cycles are acting on the turbine for each damping ratio input value, the magnitude of these stress cycles is reduced with increased damping, similar to the effects shown in Figure 4. This reduced cycle amplitude translates to a greater cycles-to-failure value, N_i , in the Palmgren-Miner eqn (3), which lowers the damage value. For all operational cases, the maximum reduction in damage occurs for significant wave heights of 0 and 2 m, conditions for which FA loading governs fatigue. This is in the same way due to the

Table 9. Percent reduction in average one-hour damage accumulation for several combinations of wind speed, significant wave height and damping ratio as compared to damage for a 1% damping ratio.

		Damping Ratio, %				
		1	2	3	4	5
		Wind Speed 3 m/s (cut-in; operational)				
Significant Wave Height, m	0	2.0e-11	24%	15%	30%	47%
	2	5.2e-07	11%	18%	24%	29%
	4	3.4e-06	8%	14%	18%	21%
	6	1.3e-05	4%	8%	12%	14%
	8	3.6e-05	3%	7%	10%	12%
		Wind Speed 11.4 m/s (rated; operational)				
Significant Wave Height, m	0	9.4e-06	6%	10%	14%	17%
	2	2.2e-05	5%	9%	12%	16%
	4	4.5e-05	4%	8%	10%	13%
	6	8.0e-05	3%	6%	8%	10%
	8	1.4e-04	2%	5%	6%	7%
		Wind Speed 25 m/s (cut-out; operational)				
Significant Wave Height, m	0	2.0e-05	11%	20%	26%	31%
	2	3.1e-05	10%	17%	23%	28%
	4	5.1e-05	7%	11%	16%	20%
	6	8.1e-05	6%	11%	15%	19%
	8	1.3e-04	5%	10%	13%	15%
		Wind Speed 30 m/s (parked and feathered; non-operational)				
Significant Wave Height, m	0	5.5e-06	18%	31%	40%	49%
	2	5.6e-06	18%	31%	41%	50%
	4	1.4e-05	38%	55%	64%	69%
	6	3.7e-05	33%	46%	54%	59%
	8	7.7e-05	28%	40%	46%	50%

importance of this relationship is illustrated by calculating the relative contributions to total damage associated with different stress amplitudes percentiles as shown in Table 10. These results are specific to the circumferential orientation calculated to have maximum damage for each combination of wind speed and significant wave height, and reflect average contributions across all wind speeds, wave heights, and damping ratios. The results in the table show how high amplitude stresses have a significantly greater contribution to damage than low amplitude stresses and further shows the significance of decreasing stress amplitude by increasing damping; a small decrease in stress amplitude can translate to a large decrease in damage and large increase in fatigue life.

Table 10. Average contribution of top percentiles of stress amplitude to accumulated fatigue damage for all combinations of wind speed, wave height and damping ratio

Stress Amplitudes	Percent contribution to Total Damage	Ratio of Stress Amplitude Percentile to Damage Contribution
Top 10%	18%	1.8
Top 20%	30%	1.5
Top 30%	48%	1.6
Top 40%	66%	1.6
Top 50%	82%	1.6

5. CONCLUSION

Increased damping decreases both the resultant mudline moment and the accumulation of fatigue damage in every combination of wind, wave, and operating conditions considered here. Resultant moments experience reductions up to 4.2% in the operating cases and up to 17.3% in the parked and feathered cases with a damping ratio increase from 1%–5%. Fatigue damage accumulation experiences reductions up to 47% in the operating cases and up to 69% in the parked and feathered cases with a damping ratio increase from 1%–5%. Greater damage reduction was experienced in the parked and feathered cases due to the lack of aerodynamic damping from the spinning blades, which allowed for foundation damping to account for a greater portion of total system damping. The larger reductions in moment and damage for the parked and feathered cases are important for storm and hurricane events. The primary reason why the prediction of fatigue damage is more sensitive to damping ratio than the resultant moment is because fatigue damage is a function of fatigue life, and the relationship between stress (which is proportional to moment) and fatigue life is nonlinear.

Only co-directional wind and waves were considered, but a similar parameter study including misalignment may demonstrate foundation damping's role in demand reduction even more strongly; misaligned wave loading would not be reduced by aerodynamic damping, so increased foundation damping would have a greater effect on total system damping similarly to the parked and feathered conditions presented in this study. It is also recommended that this research be extended to turbine lifetime simulations so that the comparison of damage values to the usage factor is possible.

By taking into account foundation damping in offshore wind turbine design guidelines, design demands in terms of both ultimate and fatigue loads can be reduced. This concept is an important factor in attacking the high capital cost barrier that hinders development of offshore wind in the United States. If it can be properly incorporated into design, it's possible that more efficient and less expensive turbines can be constructed.

6. ACKNOWLEDGEMENTS

This work is partially supported by the NSF-sponsored IGERT: Offshore Wind Energy Engineering, Environmental Science, and Policy (Grant Number 1068864), the NSF-sponsored Civil, Mechanical and Manufacturing Innovation (CMMI) Division (Grant Numbers 1234560 and 1234656), and the Massachusetts Clean Energy Center (MCEC).

REFERENCES

- [1] ABS, 2010. Guide for Building and Classing Offshore Wind Turbine Installations. Houston, TX: American Bureau of Shipping.
- [2] Carswell, W., Johansson, J., Løvholt, F., Arwade, S.R., Madshus, C., DeGroot, D.J., Myers, A.T., 2015. Foundation Damping and the Dynamics of Offshore Wind Turbine Monopiles. *Renewable Energy* 80: p. 724–736.
- [3] Chopra, A.K., 2007. Dynamics of structures: theory and applications to earth- quake engineering. 3rd ed. Upper Saddle River, NJ: Pearson Prentice Hall.
- [4] Damgaard M., Andersen J., Ibsen, L.B., Andersen L., 2012. Natural frequency and damping estimation of an offshore wind turbine structure. *Proceedings of the twenty-second international offshore and polar engineering conference*, vol. 4: p. 300-307.
- [5] DNV, 2009. Offshore Standard DNV-OS-J101: *Design of Offshore Wind Turbine Structures*. Norway: Det Norske Veritas.
- [6] DNV, 2005. Recommended Practice DNV-RPC203: *Fatigue Design of Offshore Steel Structures*. Norway: Det Norske Veritas.
- [7] IEC 61400-3, 2009. *Design Requirements for Offshore Wind Turbines*. International Electrotechnical Commission.
- [8] International Renewable Energy Agency, 2012. *Renewable Energy Technologies: Cost Analysis Series*.

- [9] Jonkman, J., Buhl, M.J., 2005. *FAST user's guide*. Golden, CO.
- [10] Jonkman, J., Butterfield, S., Musial, W., Scott, G., 2009. *Definition of a 5-MW reference wind turbine for offshore system development*.
- [11] Macaskill, A., Mitchell, P., 2013. Offshore Wind - an Overview. *WIREs Energy Environment*, 2: p. 374–383.
- [12] Manwell, J.F., McGowan, J.G., Rogers, A.L., 2009. *Wind energy explained*. 2nd ed. New York: John Wiley & Sons, Ltd.
- [13] Musial, W., Ram, B., 2010. *Large-scale offshore wind power in the United States: assessment of opportunities and barriers*, Golden, CO.
- [14] Myers, A. T., Arwade, S.R., Valamanesh, V., Hallowell, S., Carswell, W., 2015. Strength, Stiffness, Resonance and the Design of Offshore Wind Turbine Monopiles. *Engineering Structures* 100: p. 332–341.
- [15] Shirzadeh, R., Devriendt, C., Bidakhvidi, M., Guillaume, P., 2013. Experimental and computational damping estimation of an offshore wind turbine on a monopile foundation. *Journal of Wind Engineering and Industrial Aerodynamics*, Sep., 120: p. 96-106.
- [16] Stansby, P.K., Stallard, T.J., Devaney, L.C., 2013. Breaking Wave Loads on Monopiles for Offshore Wind Turbines and Estimation of Extreme Overturning Moment. *IET Renewable Power Generation* 7(5): p. 514–520.
- [17] U.S. Department of Energy, 2015. *Wind Vision: A New Era for Wind Power in the United States*.
- [18] Valamanesh, V., Myers, A.T., 2014. Aerodynamic damping and seismic response of horizontal axis wind turbine towers. *Journal of Structural Engineering*, p. 140-151.
- [19] Versteijlen, W., Metrikine, A., Hoving, J., Smid, E., de Vries, W., 2011. Estimation of the vibration decrement of an offshore wind turbine support structure caused by its interaction with soil. *EWEA offshore conference*.

